Detailed mechanical characterization of the transition zone: new insight into the integration between the annulus and nucleus of the intervertebral disc

Javad Tavakoli, Joanne L. Tipper

Centre for Health Technologies, School of Biomedical Engineering, Faculty of Engineering and Information Technology, University of Technology Sydney, NSW, Australia

*Corresponding authors: Joanne L. Tipper (joanne.tipper@uts.edu.au) and Javad Tavakoli (javad.tavakoli@uts.edu.au)

Abstract

The Nucleus Pulposus (NP) and Annulus Fibrous (AF) are two primary regions of the intervertebral disc (IVD). The interface between the AF and NP, where the gradual transition in structure and type of fibers are observed, is known as the Transition Zone (TZ). Recent structural studies have shown that the TZ contains organized fibers that appear to connect the NP to the AF. However, the mechanical characteristics of the TZ are yet to be explored. The current study aimed to investigate the mechanical properties of the TZ at the anterolateral (AL) and posterolateral (PL) regions in both radial and circumferential directions of loading using ovine IVDs (N=28). Young's and toe moduli, maximum stress, failure strain, strain at maximum stress, and toughness were calculated mechanical parameters. The findings from this study revealed that the mechanical properties of the TZ, including young's modulus ($p = 0.001$), failure strain ($p < 0.001$), strain at maximum stress ($p = 0.002$), toughness ($p = 0.027$), and toe modulus ($p = 0.005$), were significantly lower for the PL compared to the AL region. Maximum stress was not significantly different between the PL and AL regions ($p = 0.164$). We found that maximum stress ($p = 0.002$), failure strain ($p < 0.001$), and toughness ($p = 0.001$) were significantly different in different loading directions. No significant differences for modulus (young's; $p = 0.169$ and toe; $p = 0.352$) and strain at maximum stress ($p = 0.727$) were found between the radial and circumferential loading directions.

Keywords:

Intervertebral disc, transition zone, mechanical properties, annuls-nucleus boundary,

1. Introduction

The intervertebral disc (IVD), located between adjacent vertebral bodies in the spine, provides flexibility to the spinal column, plays a significant role in spinal motion, and undergoes large deformations during daily activities. The Nucleus Pulposus (NP) and Annulus Fibrous (AF) are two primary regions of the IVD. The NP, a gel-like material at the center of IVD, is a highly hydrated tissue that mainly contains collagen type II and proteoglycan [1, 2]. It is surrounded by the AF which consists of concentric annular layers, known as lamellae. Within the AF, parallel arrays of collagen type I fibers are organized at alternating angles creating a highly packed and well-organized tissue [3]. The AF – NP interface, where a gradual transition from collagen type I to type II is observed, is known as the Transition Zone (TZ) [4].

Compared to the AF and NP, few studies have attempted to characterize the TZ region in the IVD. These studies mainly focused on understanding the structural architecture and biological activity of the TZ region and its mechanical properties (including modulus, toughness, maximum stress, failure strain, and failure at maximum stress) have not been previously explored [5-11]. There has been only one study published on the mechanical integration between the NP and surrounding AF using ovine IVDs, indicating that the TZ could support a load range of 2 – 11.5 N [5]. In this study, sagittal tissue slabs (vertebra-IVD-vertebra with a thickness of ≈10 mm) were dissected from the IVD central portion and the entire endplate (top and bottom) adjacent to the NP was removed. The results from the uniaxial tension tests were reported as raw load-displacement curves since accurate measurement of the load-bearing area was not possible. Indeed, this study utilized formalin-fixed samples to visualize the TZ fibers' deformation in response to tension [5]. Since mechanical properties of the TZ region are not known, current computational and tissue-engineered IVD models are less clinically relevant as they are unlikely to reflect accurate mechanical integration between the AF and NP. By improving our knowledge about the nature of the AF-NP integration, it is possible to explore

how the TZ accommodates the NP shape changes during IVD bulging and investigate its contribution to the initiation of herniation and IVD failure which is important for clinical studies.

Early IVD studies considered the NP as an isolated entity that was separated from the AF with unspecified boundaries. Despite the fact that the NP was contained by the AF, these studies concluded that the connection between these regions was formed via randomly organized fibers and therefore, there was no significant mechanical interaction between the regions [12, 13]. Several studies revealed various structural and biological characteristics of the TZ region by investigating its structural architecture using light [5-7] or scanning electron microscopes [8] and exploring its metabolic activity [9, 10].

Attempts to characterize the TZ structural organization using a light microscope revealed a criss-cross pattern for the elastic fibers [6, 7]. In addition, the TZ was reported to connect the NP to the inner AF via a network of fibers supporting an average uniaxial tensile load of 5.7 N [5]. Our recent ultrastructural studies utilized extracellular matrix digestion to visualize the organization of elastic fibers at the TZ region and identified a dense and well-organized elastic network conferring a significant degree of radial interconnectivity between the AF and NP [8, 14]. Indeed, parallel elastic fibers in the NP that were running towards the AF merged to form an elastic network at the TZ [15]. These structural studies suggested a mechanical role for the TZ region through the establishment of a highly integrated fibrous network that spans the NP and anchors into the inner AF. Unfortunately, the mechanical properties of the TZ are not fully understood and whether this region plays a role in IVD herniation and degeneration is yet to be determined. Different parameters including loading conditions (rate, magnitude, direction), age, and health situation influence the mechanism and extent of IVD failure. Extensive studies have been performed to understand how IVDs fail under different conditions and have identified that endplate fracture and AF rupture are two common modes of IVD failure [16-

23]. A clinical study examined herniated IVDs from 181 patients and observed that endplate fracture was twice as likely to occur compared to AF disruption [23]. A biomechanical study utilized ovine IVDs to create herniation in vitro and revealed that the exposure of IVD to physiological compression combined with lateral bending and flexion led to endplate fracture in 76% of specimens and AF failure in 24% of specimens [16]. Endplate fracture was also reported in another study that exposed human IVDs to the combination of repetitive complex loading (flexion, axial rotation, and compression) for 20,000 cycles [24]. Healthy IVDs have been shown to fail in the outer AF when they are exposed to combined flexion and compression [17, 18]. Damages to the AF included direct radial, circumferential, and lateral tears as well as AF-endplate failure [19-22]. Although these studies have enhanced our knowledge about IVD failure under various conditions, how the TZ region may contribute to the IVD failure has remained unclear.

During IVD aging and degeneration the TZ region is extremely difficult to define. Studies have shown that the NP becomes fibrotic and less distinct from the AF region which is related to the loss of water. Accordingly, clefts are developed at the AF and NP junction (TZ region) to separate the NP from the AF. This gradual degeneration process turns the NP into a solid and dry mass and reduces its ability to redistribute and transmit intradiscal load which significantly weakens the overall IVD strength [25-28]. This observation may indicate the impact of the TZ on the microstructural integrity of the IVD.

Apart from the impact of the TZ region on the structural integrity of the IVD and the associated mechanical changes during aging and degeneration, biological studies have identified the TZ region of maximum metabolic activity using animal (porcine and rabbit) IVD models [29-32]. The TZ region likely represents the growth plate of the NP [3, 33]. In addition, it was observed that cell morphology and mechanics are significantly different for the TZ compared to the NP region. The NP cells were approximately 3 times stiffer and significantly more viscous than

the cells in the TZ [11]. These observations may be related to the cytoskeletal architecture of the TZ cells and the mechanical properties and structural hierarchy of the TZ tissue, indicating its likely role in the developmental biology and degeneration of IVD.

Motivated by emerging information of the biological role of the TZ region and its plausible impact on the structural integrity between the AF and NP, the current study aimed to explore the mechanical properties of the TZ at the anterolateral (AL) and posterolateral (PL) regions in both radial and circumferential directions of loading using ovine IVDs. We hypothesized that the TZ mechanical strength is lower at the PL, compared to the AL region, and the TZ region exhibits different mechanical strength in the radial compared to the circumferential directions of loading. Both hypotheses were proposed based on our previously published structural study where we found an orthotropic structure for the TZ elastic network and, in addition, the thickness of the elastic fibers in the PL region were smaller (< 200 nm) compared to those that were located in the AL region (≈ 1 μm) [8]. From a clinical point of view, the NP is a heterogeneous structure and is loaded in multi directions when the IVD is exposed to different types of loading; hence, it is likely that the TZ region is loaded in both radial and circumferential directions. Therefore, it is important to identify the mechanical properties of the TZ region in both directions.

2. Materials and Method

2.1.Assistive devices for sample preparation:

Two assistive custom-made devices including a double-blade cutter and paper-based labeler were prepared to facilitate sample preparation. The custom-made double-blade cutting device was made by placing two plexiglass cuboids (L = 5 × W = 5 × t = 5 mm) between two feather trimming blades (No 260 L, Feather safety razor Co. Ltd, Japan). Trimming blades were 5 mm apart and therefore allowed us to dissect tissue blocks with 5 mm width. The plexiglass cuboids

were prepared using a laser cutter (Epilog Fusion M2, Alfexlaser). The same strategy was recruited using 1 mm thick plexiglass cuboids to develop a double-blade cutting device to prepare samples with 1 mm thick. Photo paper strips (Kodak 180 mg; L = 15 mm × W = 5 mm) were used to prepare the paper-based labeling device. Two rectangles (L = 3 mm × W = 4 mm) with a 1 mm distance apart were cut from the stips using a laser cutter. Moving the labeling device over the surface of each sample, under microscopic observation, enabled us to identify the region of interest for mechanical testing.

2.2.Sample preparation

Fresh frozen ovine spines (N = 28) were obtained from a local abattoir and L4/5 IVDs, dissected from the vertebrae, were used for sample preparation (Fig 1a). IVDs were then randomly categorized into four different groups (Figs 1b, 1c) of AL-radial, AL-circumferential, PL-radial, and PL-circumferential (N = 7 IVDs in each group). While frozen, blocks of IVD tissue were cut from the AL and PL regions of the IVD in both radial and circumferential directions, as denoted by red (radial) and black (circumferential) rectangles in Fig 1d using the custom-made double-blade cutting device. The circumferential tissue blocks, from the AL and PL regions, were dissected from adjacent to the last layer of the inner AF using a stereomicroscope (RL-M3, China). In our previously published study, a 5 mm distance from the last layer of the inner AF towards the NP was considered to represent the state of the TZ [8]. Within this region, we found a different structural organization for the TZ elastic fibers compared to the rest of the NP [15]. Therefore, the width of the tissue blocks was set to 5 mm to ensure that the TZ region was selected and the effect of the AF lamellae and NP on sample preparation was minimal. Tissue blocks were then attached on the top of a plexiglass sheet using cyanoacrylate adhesive and placed in the freezer (-18ºC for 1 hr). Samples with 1mm thickness were then sliced (transversely) from the middle of the frozen tissue blocks (Figure 1e) using the double-blade cutting device (1 mm distance between blades). The average width

and thickness of the samples were 5.3 ± 0.5 and 1.2 ± 0.3 mm, respectively (sample length ≈ 10 -15 mm). The length of the samples was not accurately measured since the effective area to calculate mechanical parameters was determined by the width and thickness of the samples.

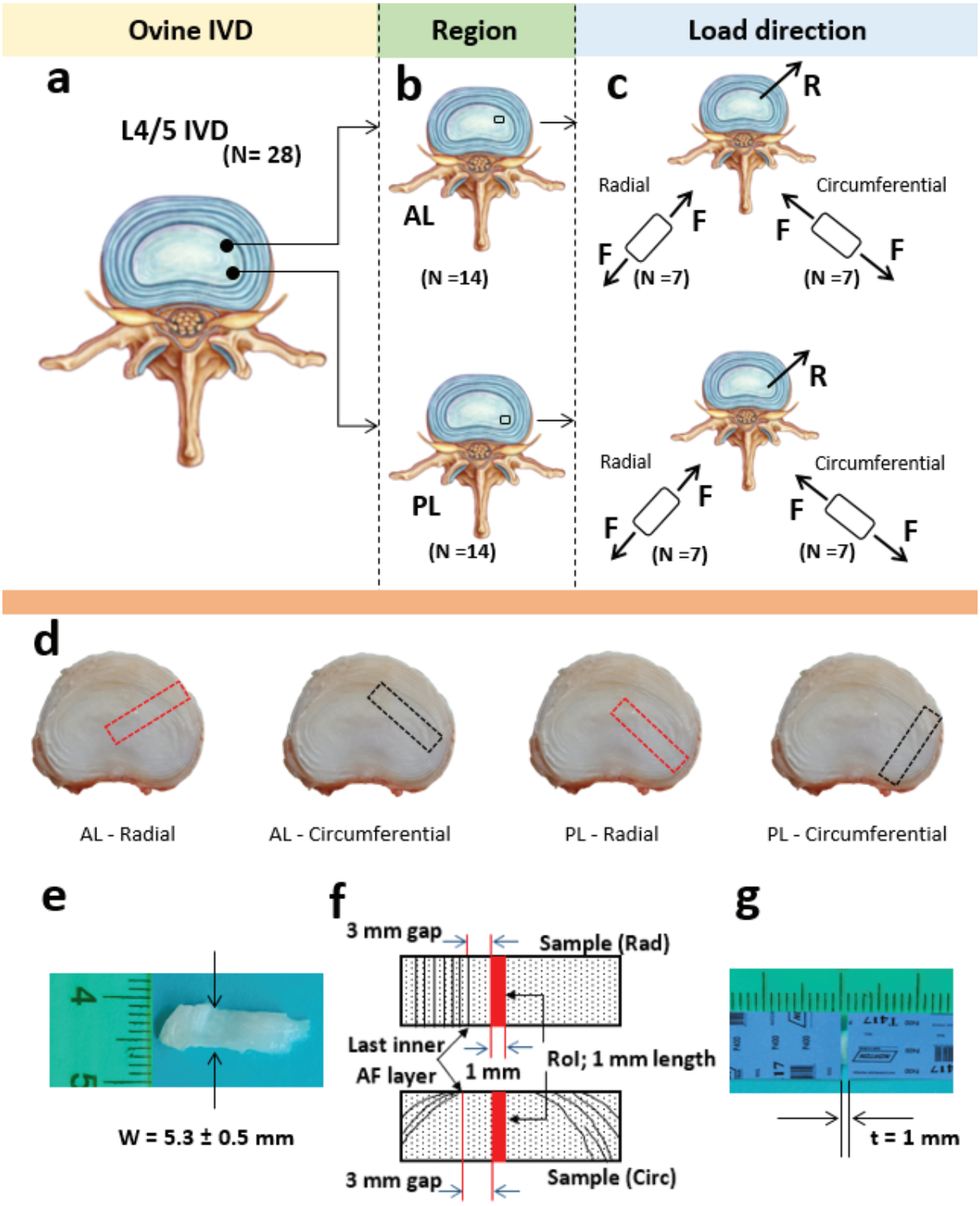

Figure 1- Sample preparation. (a) Dissected L4/5 IVDs were used for sample preparation and (b, c) based on the region of interest and load direction were categorized into four different groups of AL-radial, AL-circumferential, PL-radial, and PL-circumferential (N = 7 IVDs in each group). (d) Blocks of IVD tissue (average width = 5.3 ± 0.5 and thickness = 1.2 ± 0.3 mm) were cut from the AL and PL regions of the IVD in both radial and circumferential directions, as denoted by red (radial) and black (circumferential) rectangles. (e) Samples with 1mm thickness were then sliced from the block tissues. (f) A distance of 3 mm from the last layer of the inner AF towards the NP was considered as the region of interest (TZ) for mechanical testing. (g) Adjacent to the 3 mm gap distance, a region with 1 mm length was identified and sandpaper was attached to each edge (above and below) using cyanoacrylate adhesive.

2.3. Sample preparation for mechanical testing

Sample preparation for mechanical testing was performed under a microscopic observation (RL-M3T stereo microscope, China) using the same methodology that was developed for the measurement of the mechanical properties of the interlamellar matrix in the AF [34, 35]. A distance of 3 mm from the last layer of the AF towards the NP (Fig 1e) was considered as the region of interest (TZ) to prepare samples for mechanical testing. Adjacent to the 3 mm gap, a region with 1 mm length was identified as accurately as possible using the assistive paper-based labeling device (Fig 1f). Under microscopic observation, the assistive device was moved over the surface of each sample and a permanent marker was used to fill two rectangles (L = 3 mm × W = 4 mm) to identify the region of interest. Sandpaper (400 grit) was attached to the edge (above and below) of the filled-by-marker regions using cyanoacrylate adhesive (Fig 1g). This strategy for sample preparation was consistent among all samples. It is important to note that although extra care was paid to cut circumferential samples close to the last layer of the inner AF, due to the IVD curvature some AF layers were still partially present at both edges of

the samples (Fig 1f). Considering a 3 mm distance from the last AF layer allowed us to select the region of interest from where the AF layers were not observed.

2.4. Mechanical testing

All samples (4 groups AL-radial, AL-circumferential, PL-radial, and PL-circumferential; N = 7 samples in each group) were initially equilibrated in 0.15M phosphate buffer saline (PBS) at room temperature for 5 min. A 5 min swelling protocol was chosen to minimize potential NP materials (i.e. glycosaminoglycans) leaching with time, and therefore the impact of free swelling on the NP material properties was negligible [36]. Each sample was subjected to failure mechanical tests (radial and circumferential) using an Electroforce testing machine (Biodynamic 5100, load cell capacity = 22 N (1% full-scale accuracy), TA Instruments, USA) at a displacement rate of 0.1 $mm.s^{-1}$ (strain rate= $10\%s^{-1}$). In our previously published study, we used reported human IVD deformation and pressure data and identified that the relevant physiological strain rate in the radial direction was approximately $7\%s^{-1}$ [34, 37-41]. Considering the limitation of the Electroforce testing machine (displacement limits = ± 6.5 mm), our preliminary results showed that the TZ failure was unlikely to occur at lower strain rates ($< 7\%s^{-1}$). On the other hand, in our previously published study, we observed that the ILM failed under $10\%s^{-1}$ strain rate [33]; hence, we chose a strain rate of $10\%s^{-1}$ to perform mechanical testing in the current study where the TZ failure was most likely to occur. In addition, this strategy may help to understand the mechanical behavior of the TZ region under injury conditions, since the TZ was exposed to a higher than physiological strain rate.

2.5.Data and statistical analysis

Engineering stress-strain curves were used to characterize the mechanical properties of the TZ region. Outcome measures (Fig 2) of young's and toe moduli, maximum stress, failure strain, and toughness were calculated using Matlab (R2021a, The Mathworks Inc.). Maximum stress

was defined as the peak stress that was recorded during the test and failure strain was considered as the maximum strain that the sample experienced before being fully disintegrated. Modulus was calculated as the slope of the best-fit line to the stress-strain curve with toe modulus representing the initial region of the failure test. The moving cell linear regression method was used to determine the most linear region and calculate young's and toe moduli. Both moduli were defined by the regression line with the largest coefficient of determination (r^2), while the regression commenced at zero strain and 70% of maximum stress for toe and young's modulus, respectively [42-44]. Within the toe region, fibrous elements of the tissue were most likely to be uncoiled while young's modulus represented the region where the majority of fibers in the TZ region were fully recruited. Toughness was the area under the stress-strain curve.

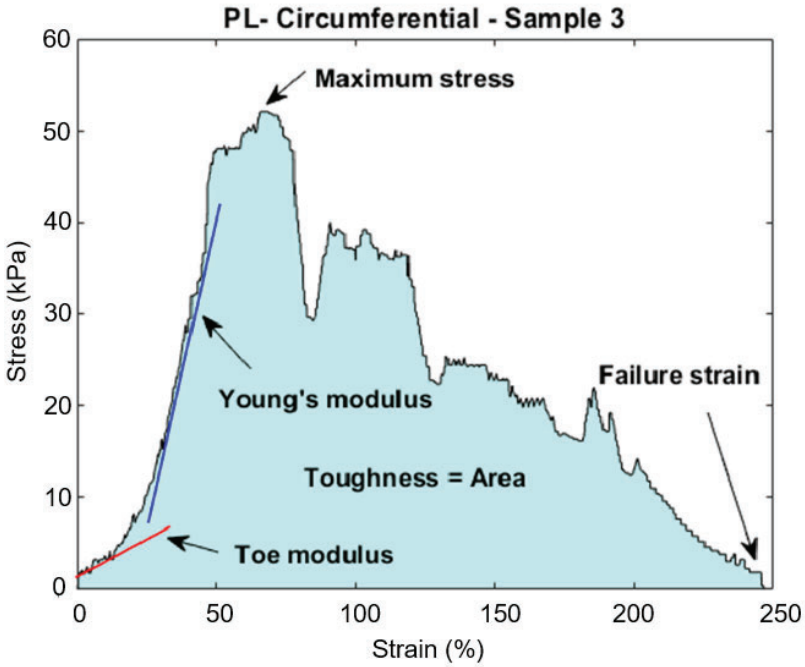

Figure 2 – Identification of mechanical parameters that were calculated to characterize the TZ region of the IVD. Stress-strain curve for a sample that was harvested from the PL region of the IVD and mechanically tested in the circumferential direction.

For statistical analysis, all data were first assessed for normality using Kolmogorov-Smirnov and Shapiro-Wilk test. To identify the statistical differences for the mechanical parameters between regions and load directions, separate two-way ANOVA and Mann-Whitney U tests were conducted for normally and non-normally distributed data, respectively. Statistical power analysis, with alpha = 0.05 and sample size = 7, was performed to determine the sample size effect.

3. Results

The results of the Shapiro-Wilk test revealed that the data for young's modulus ($p = 0.064$), failure strain ($p = 0.168$), and strain at maximum stress ($p = 0.212$) were normally distributed ($p > 0.05$). On the other hand, the data for toe modulus ($p = 0.032$), toughness ($p = 0.019$), and maximum stress ($p = 0.038$) were not normally distributed ($p < 0.05$). Engineering stress-strain curves were prepared for all sample groups (Supplementary file) and were used to calculate the mechanical properties of the TZ region. Typical TZ stress-strain curves for four sample groups (Figure 3) revealed a small toe region followed by a rapid increase to maximum stress. Moreover, an irregular decay in stress to eventual failure was observed for all samples.

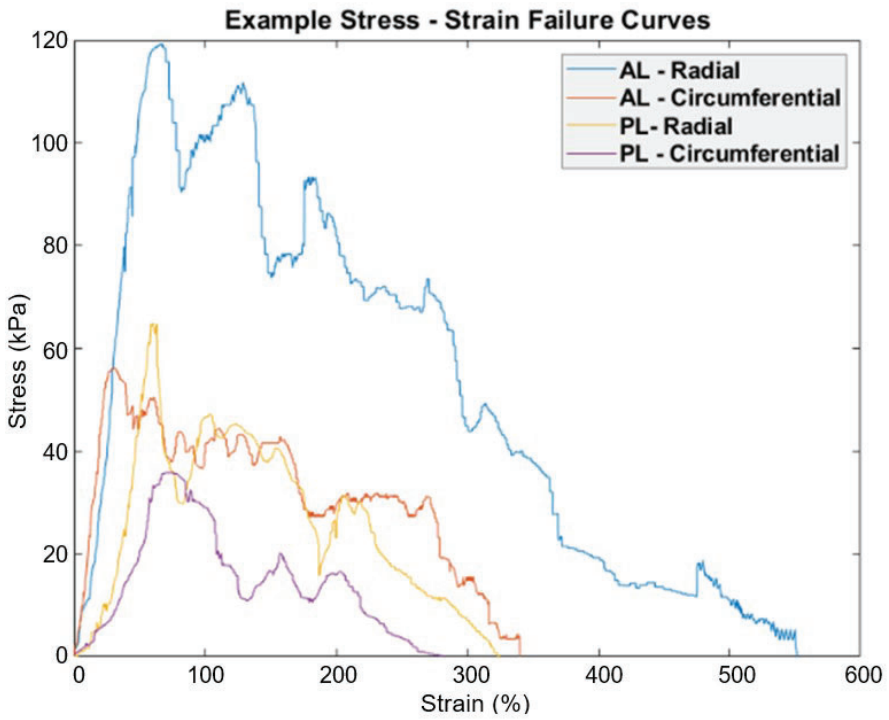

Figure 3- Example TZ stress-strain curves for all four sample groups including samples that were harvested from the anterolateral (AL) and posterolateral (PL) regions and were tested in radial and circumferential directions.

Statistical analysis for the calculated mechanical properties, including young's modulus, failure strain, strain at maximum stress, maximum stress, toughness, and toe modulus are described as follows:

3.1. Young's modulus

The mean (± 95% CI) TZ young's moduli were 0.30 (± 0.08) and 0.31 (± 0.16) kPa for the AL region in radial and circumferential directions, respectively (Supplementary file). The mean (± %95 CI) TZ young's moduli for the PL region were 0.22 (± 0.10) and 0.09 (± 0.05) kPa in radial and circumferential directions, respectively (Fig 4a).

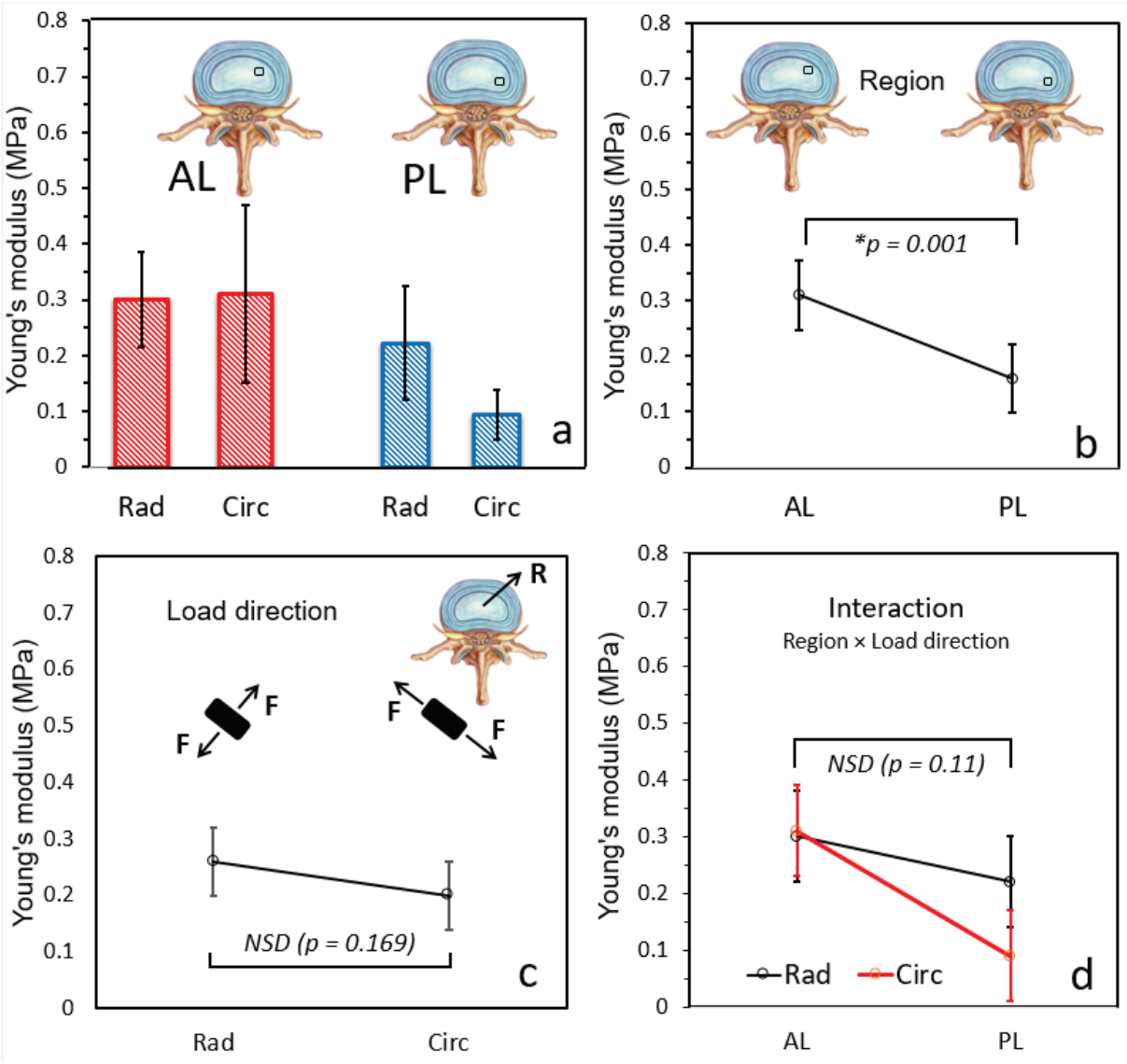

Figure 4 – (a) Comparison of the mean (± 95% CI) young's modulus for anterolateral (AL) and posterolateral (PL) regions in radial and circumferential loading directions and summary of ANOVA results for (b) region, (c) load direction and (d) region × load direction interaction.

The overall effect of region for young's modulus was significant (p = 0.001). It was observed that young's modulus of the PL region was significantly lower than the AL region. However, there was no significant difference in young's modulus for the radial compared to the circumferential loading direction (p = 0.169) and for the region×load direction interaction (p = 0.1192) (Figs 4b – 4d).

3.2. Failure strain

The mean (± 95% CI) TZ failure strains were 4646.3 (± 619.7) and 3590.7 (± 393.9) mm/mm in the radial direction of loading for the AL and PL regions, respectively (Supplementary file). It was found that the mean (± 95% CI) TZ failure strains were 3465 (± 501.7) and 2783.6 (± 250.4) mm/mm in the circumferential direction of loading for the AL and PL region, respectively (Fig 5a). The overall effects of region and load direction were significant ($p < 0.001$), indicating that the TZ failure strain was significantly smaller for the PL compared to the AL region and in the circumferential compared to the radial direction of loading. Nevertheless, the overall effect of region × load direction interaction ($p = 0.292$) was not significant (Figs 5b – 5d).

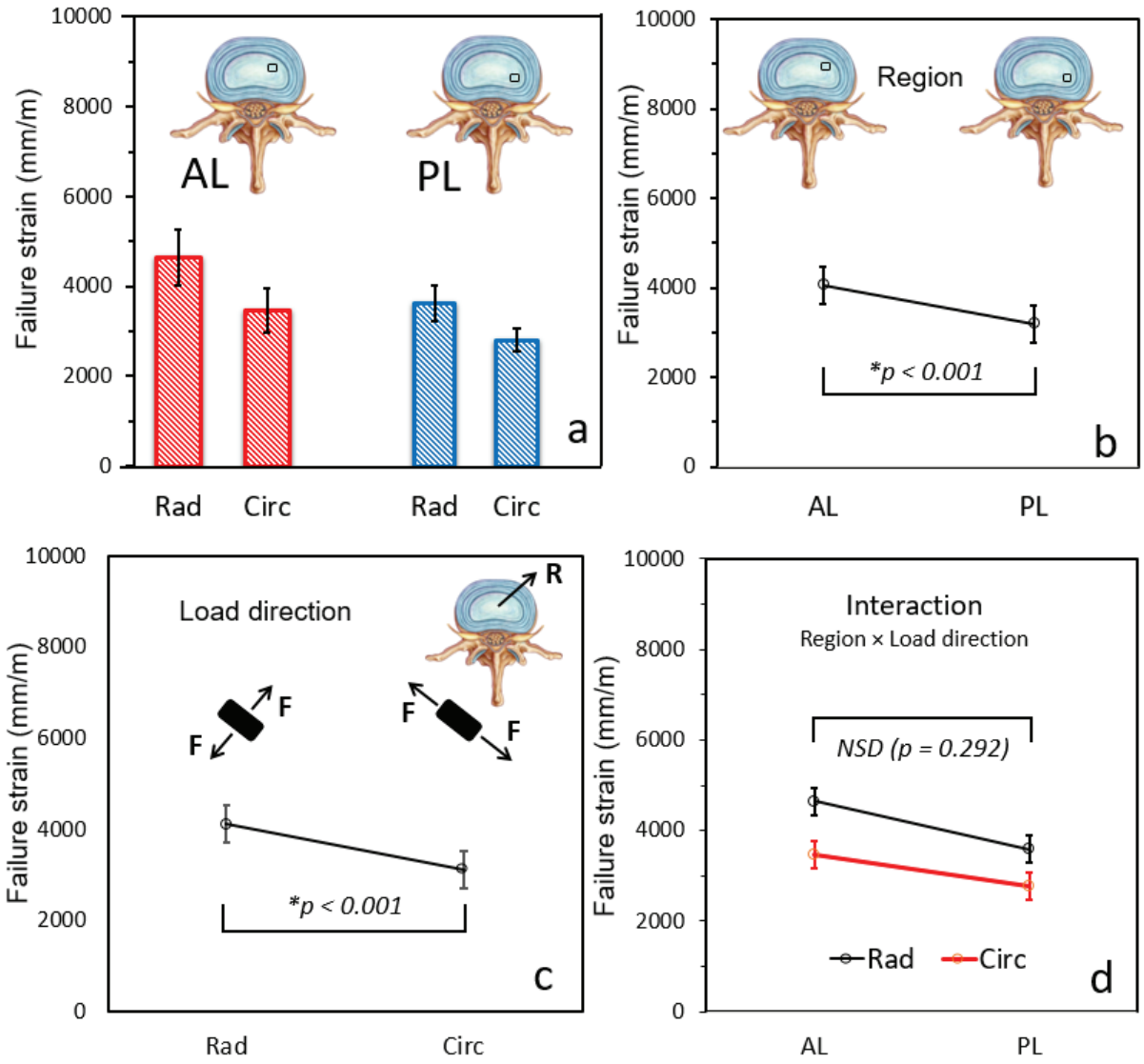

Figure 5 – (a) Comparison of the mean (± 95% CI) failure strain for anterolateral (AL) and posterolateral (PL) regions in radial and circumferential loading directions and summary of ANOVA results for (b) region, (c) load direction and (d) region × load direction interaction.

3.3. Strain at maximum stress

The mean (± 95% CI) TZ strains at maximum stress were 641.8 (± 103.4) and 689.3 (± 99.4) mm/mm in the radial direction of loading for the AL and PL regions, respectively (Supplementary file). It was found that the mean (± 95% CI) TZ strains at maximum stress were 502.7 (± 201.8) and 799.1 (± 90.7) mm/mm in the circumferential direction of loading for the AL and PL region, respectively (Fig 5a). There was a statistically significant interaction

between the effect of load direction and region on strain at maximum stress for the TZ region ($p = 0.020$). Simple main effect analysis showed that the effect of the region was significant ($p = 0.002$) and a lower strain at maximum stress was observed for the AL compared to the PL region ($p = 0.002$); however, there were no significant differences between different load directions ($p = 0.772$).

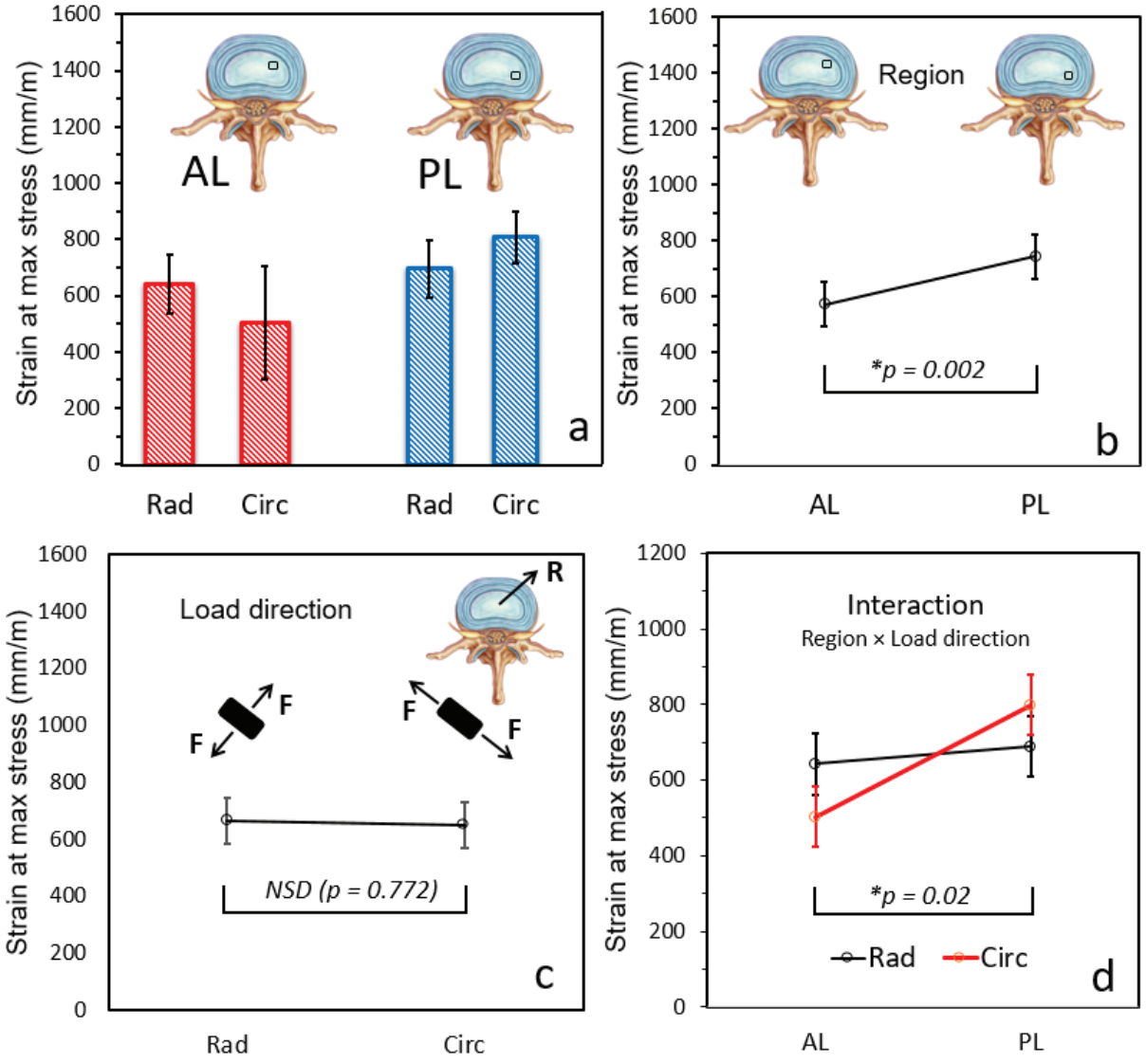

Figure 6 – (a) Comparison of the mean (± 95% CI) strain at maximum stress for anterolateral (AL) and posterolateral (PL) regions in radial and circumferential loading directions and summary of ANOVA results for (b) region, (c) load direction and (d) region × load direction interaction.

As explained before, the data for maximum stress, toughness, and toe modulus were not normally distributed; hence, the Mann-Whitney U test was used to identify significant differences.

3.4. Maximum stress

The mean (± 95% CI) TZ maximum stresses were 90.2 (± 21.3) and 66.4 (± 14.7) kPa for the AL and PL region, respectively (Supplementary file). It was also observed that the mean (± %95 CI) TZ maximum stresses in the radial and circumferential directions of loading were 96.8 (± 19.4) and 59.8 (± 13.2) kPa, respectively (Figs 7a and 7b). According to the Mann-Whitney test, there was no significant difference for the Mean Rank between the AL (16.7) and PL (12.3) regions (p = 0.164). However, the Mean Rank between the radial (19.2) and circumferential (9.8) direction of loading was significantly different, indicating that the maximum stress was significantly lower in the circumferential compared to the radial direction of loading (p = 0.002). The scatter plots for the maximum stress by region and load direction can be found in the supplementary file.

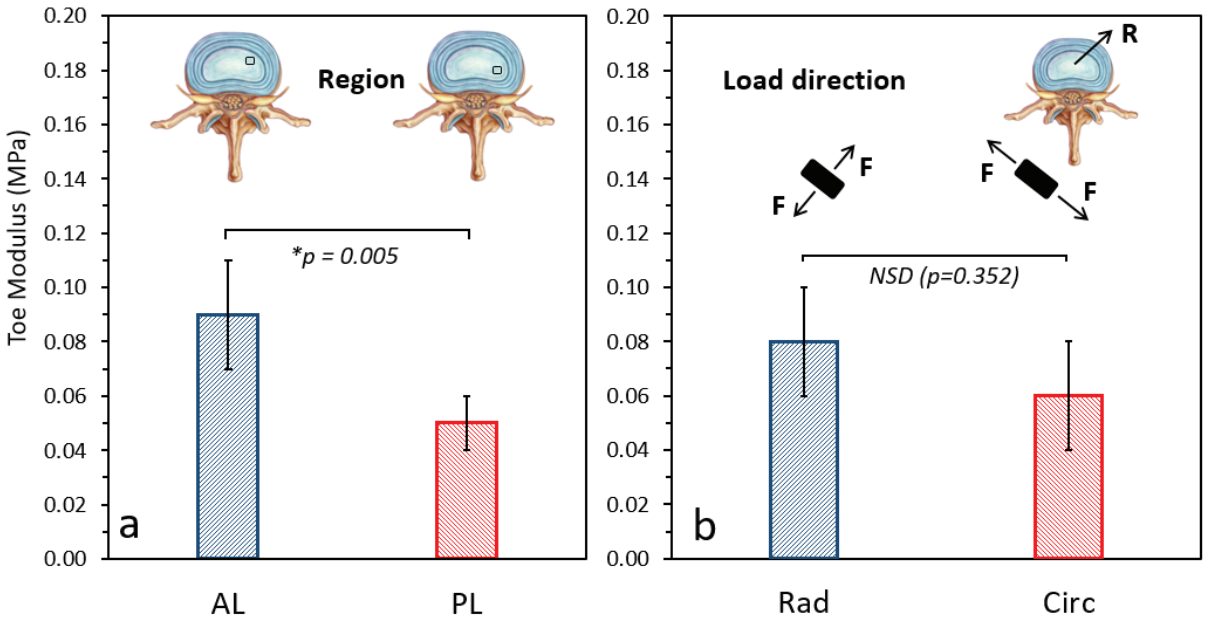

Figure 7 – Comparison of the mean (±95% CI) maximum stress for the (a) anterolateral (AL) and posterolateral (PL) regions and (b) in the radial and circumferential loading directions.

3.5. Toughness

The mean (± 95% CI) TZ toughnesses were 183208.2 (± 51400) and 107082.7 (± 33200) kJ.m^{-3} for the AL and PL regions, respectively (Supplementary file). Moreover, the mean (± %95 CI) TZ toughnesses in the radial and circumferential directions of loading were 196914 (± 48400) and 93376.9 (± 52900) kPa, respectively (Figs 8a and 8b). We observed a significantly higher ($p = 0.027$) Mean Rank for toughness in the AL (17.9) compared to the PL (11.1) region, and in the radial (19.4) compared to the circumferential (9.6) loading direction ($p = 0.001$). The scatter plots for the toughness by region and load direction can be found in the supplementary file.

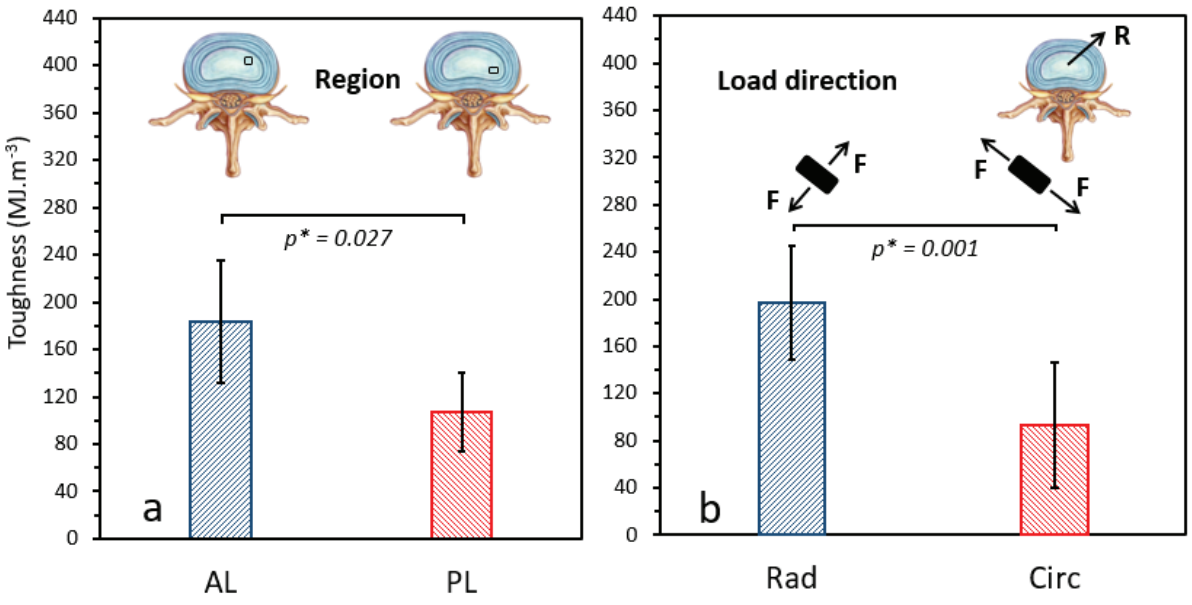

Figure 8 – Comparison of the mean (± 95% CI) toughness for (a) the anterolateral (AL) and posterolateral (PL) regions and (b) in the radial and circumferential loading directions.

3.6. Toe modulus

The mean (± 95% CI) TZ toe moduli were 0.09 (± 0.02) and 0.05 (± 0.01) kPa for the AL and PL regions, respectively (Supplementary file). The mean (± %95 CI) toe moduli for the TZ region were 0.08 (± 0.02) and 0.06 (± 0.02) kPa in the radial and circumferential loading directions, respectively (Figs 9a and 9b). We identified a significantly higher (p = 0.005) Mean Rank for toe modulus for the AL (18.7) compared to the PL (10.2) region. However, the Mean Rank for the toe modulus was not significantly different in the radial (15.9) compared to the circumferential (13.1) loading direction (p = 0.352). The scatter plots for the toe modulus by region and load direction can be found in the supplementary file.

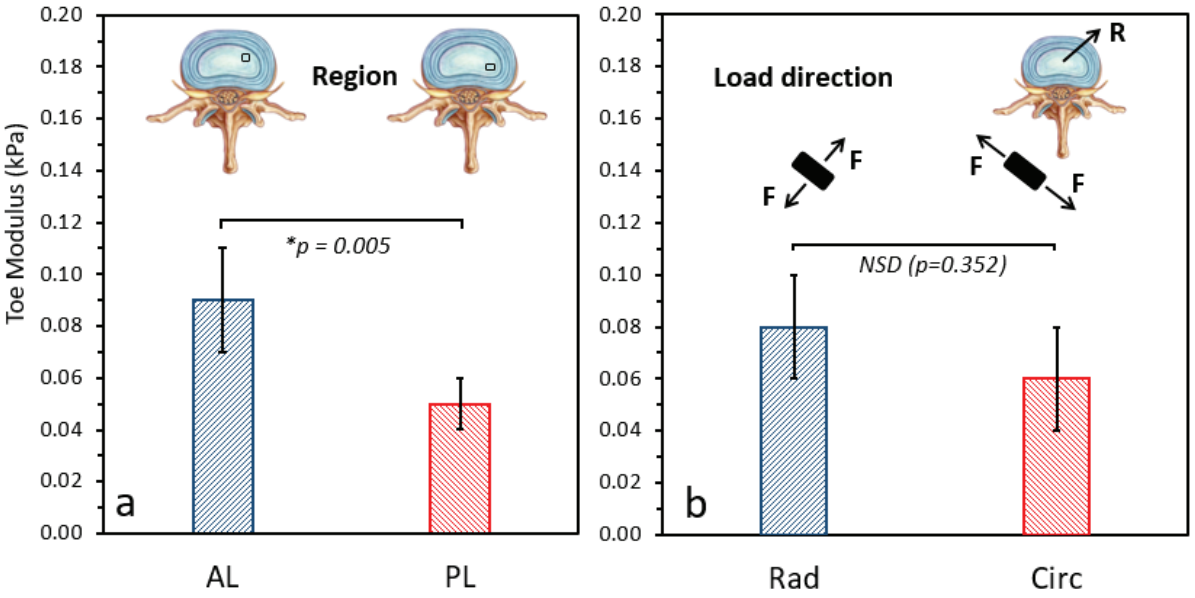

Figure 9 – Comparison of the mean (± 95% CI) toe modulus for (a) the anterolateral (AL) and posterolateral (PL) regions and (b) in the radial and circumferential loading directions.

A summary of the statistical analyses for the overall effects of the regions (AL *vs*. PL) and loading directions (radial *vs.* circumferential) is presented in Table 1.

Table 1- Summary of statistical analyses for calculated mechanical properties indicating the overall effects of the regions (AL *vs.* PL) and loading directions (radial *vs.* circumferential)

Mechanical Properties	Region	Load direction	Interaction
Two–way ANOVA test			

Young's Modulus (kPa)	*(p = 0.001)	NSD (p= 0.169)	NSD (p= 0.11)
Failure Strain (mm/mm)	* (p < 0.001)	*(p < 0.001)	NSD (p= 0.292)
Strain at max stress (mm/mm)	*(p = 0.002)	NSD (p= 0.727)	*(p = 0.02)
Mann-Whitney U test			
Mechanical Properties	**Region**	**Load direction**	
Maximum Stress (kPa)	NSD (p= 0.164)	*(p = 0.002)	
Toughness (kJ. m^{-3})	*(p = 0.027)	*(p = 0.001)	
Toe Modulus (kPa)	*(p = 0.005)	NSD (p= 0.352)	
*** significantly different**	**NSD = no significant difference**		

A summary of observed power (R^2) to identify the effect of sample size, where significant differences for mechanical parameters were found (Table 1), is presented in Table 2.

Table 2- Summary of observed power (R^2) for calculated mechanical properties.

Mechanical properties	**R^2 (Region)**	**R^2 (Loading Direction)**
Young's Modulus (kPa)	0.994	NSD
Failure Strain (mm/mm)	0.998	0.999
Strain at max stress (mm/mm)	0.867	NSD
Maximum Stress (kPa)	NSD	0.875
Toughness (kJ. m^{-3})	0.696	0.844
Toe Modulus (kPa)	0.853	NSD

As shown in Table 2, the observed power to identify the effect of sample size for young's modulus, failure strain, strain at maximum stress, and toe modulus between the AL and PL regions were 0.994, 0.998, 0.867, and 0.853, respectively. Moreover, the observed power to evaluate the effect of sample size for maximum stress, failure strain, and toughness between loading directions were 0.875, 0.999, and 0.844, respectively. The use of 7 samples in each group sample was adequate to ensure true differences would be found for the above-mentioned mechanical parameters. However, the observed power to recognize the effect of sample size for toughness between the AL and PL regions was 0.696 (Table 2). Although the Mann-Whitney results showed that the Means Rank for toughness (p = 0.027) was significantly different between the regions, the associated effect size was modest and the current sample size might not be sufficient to identify the true differences. The results of the current study revealed

that the region by itself accounted for only 21.7% (partial Eta squared; $\eta^2 = 0.217$) of the overall (effect + error) variance.

4. Discussion

The current study aimed to mechanically characterize the TZ region of the IVD during failure mechanical testing. Different mechanical parameters including young's modulus, maximum stress, failure strain, toughness, and toe modulus were calculated for the AL and PL regions of the IVD in both radial and circumferential load directions. The first challenge in the current study was to define an exact boundary between the NP and the inner layers of the AF. To tackle this challenge, sample preparation for mechanical tests was performed under a microscope and a 3 mm gap was considered between the last layer of the inner AF and the region of interest (Fig 1f). This strategy for sample preparation was consistent among all samples. Calculating strain using gripper-to-gripper distance, instead of utilizing a non-contact method, presented a limitation, however since there was no evidence of sample slippage, the measured strain was representative of global tissue strain. In addition, the use of ovine IVD may impose another limitation as human models are more clinically relevant. However, different studies have supported the use of an ovine model based on its structural and biochemical similarities to the human IVD [45-51]. Unfortunately, it was not possible to use human IVD in the current study as cadaveric specimens are often highly degenerated (grade > 3). This involves dried and fibrotic NP with clefts, which are often observed in different regions, making sample preparation difficult. The current research can be used as a pilot study to identify the mechanical characteristics of the TZ region using healthy human IVDs. It is also important to pay attention to the effect of sample size when interpreting the results of the current study. Our previous studies to characterize the structure and mechanical properties of the AF lamellae and interlamellar matrix (ILM) have recruited 6 to 10 samples where the observed powers were > 0.9 [35, 52]. The use of 7 samples in each group sample (28 samples in total) was adequate to

ensure true differences would be found. However, it was found that although toughness ($p = 0.027$) was significantly different between the AL and PL region, the effect sizes were modest (power < 0.7). The partial Eta squared for toughness was 0.217. This indicated that the region by itself accounted for only 21.7% of the overall (effect + error) variances for toughness, and therefore, a bigger sample size was required to identify the true differences for this parameter between the regions.

The findings from this study confirmed our first hypothesis that the mechanical properties of the TZ region were significantly lower for the PL compared to the AL region, except for the maximum stress (Table 1). Our second hypothesis was also partially valid, as maximum stress ($p = 0.002$), failure strain ($p < 0.001$), and toughness ($p = 0.001$) were significantly different for different loading directions (Table 1). No significant differences for modulus (young's; $p = 0.264$ and toe; $p = 0.352$) and strain at maximum stress ($p = 0.819$) were found between the radial and circumferential load direction (Table 1). The observation of lower mechanical properties for the TZ region of the IVD was consistent with other studies that have reported the occurrence of herniation posterolaterally [20, 23, 53-55]. The observation of a higher modulus for the AL compared to the PL region of the TZ indicated a greater tissue elasticity for the AL region. This was consistent with other studies that have identified similar results for the AF based on the density and organization of collagen fibers in the lamellae and stronger endplate-to-endplate connectivity [56-62]. For the TZ region, the current observation was supported by our previous findings which indicated that the elastic network in the PL region of the TZ was more delicate compared to the AL region [8]. Compared to the PL region, the elastic network in the AL consisted of major thick elastic fibers (≈ 1 μm) that were interconnected with thin (< 200 nm) elastic fibers. With the same ultrastructural organization, the thickness of the elastic fibers in the PL region was smaller (< 100 nm) compared to those that were located in the AL region [8]. These structural differences may explain the significant differences that were

observed for the toe and young's moduli between the AL and PL region of the TZ. Toe region modulus refers to the initial elasticity of crimped collagen fibers and elastic network as well as their interaction at low stretch magnitudes, which is dominated by IVD hydration, age, and degeneration state [63-65]. This suggests that mechanical properties of the toe region are likely to be important for the investigation of mechanobiological events (i.e. cell-tissue interaction) that occur at low stretch magnitudes [66, 67]. When the IVD tissue is exposed to high stretch magnitudes (such as during progression to herniation), large displacement of the NP material is likely to happen affecting the young's modulus region [54, 68].

Based on the structural differences (i.e. orientation and thickness) of the elastic network in the AL and PL regions, extensible elastic fibers are likely to assist TZ tissues in returning to their original shape after deformation. While collagen fibers are known to control the overall stiffness of IVD tissues, parallel alignment and cross-connectivity between collagen bundles and the elastic network in the TZ play an important role in the structural integrity of the IVD tissue, to further control tissue deformation and affect the overall mechanical properties [69-71].

The current study was the first of its kind to characterize the mechanical properties of the TZ and therefore it was not possible to fully compare the results with other studies. One structural study reported TZ, with full IVD thickness, could support an overall load of 5.7 N (range 2-11.5 N) [5]. The mean (± 95% CI) TZ maximum loads measured in the current study were 0.54 (± 0.2), 0.37 (± 0.2), 0.43 (± 0.1), and 0.23 (± 0.1) N for AL-radial, AL-circumferential, PL-radial, and PL-circumferential samples, respectively (Fig 5a). Considering different thicknesses between our sample (≈ 1mm) and samples in the previous study (full IVD thickness), the load magnitudes in our study were approximately 10-fold smaller compared to previously reported values. In addition, a "J" form load-extension curve up to peak load was reported in the previous study [5]. Consistent with that, our current investigation found stress-

strain curves with similar patterns for all group samples (Supplementary file). The observation of an irregular decay in stress to eventual failure for all sample groups was more likely relevant to the sub-failure of the TZ fibrous network before final failure.

Compared to our previous study that investigated the mechanical properties of the AF interlamellar matrix (ILM) in ovine IVDs, we found lower maximum stress for the TZ compared to the ILM [34]. The total mean (± 95% CI) maximum stresses for the TZ were 90.2 (± 21.3) and 66.45 (± 14.7) kPa for the AL and PL regions, while our previous studies revealed maximum stresses of 190.4 (± 78.3) and 155.9 (3± 9.1) kPa for the ILM at the anterior and PL regions, respectively. The total mean (± 95% CI) maximum stress for the AF lamella was previously reported as 249.4 (± 28.4) kPa, which was higher than that of the TZ [20, 60, 72, 73]. Compared to other studies that have reported the mechanical properties of single lamellae within the AF and NP, we found lower mechanical properties for the TZ region. The effective aggregate (confined compression) and complex (shear) moduli of non-degenerated human NP were reported as 1 MPa and 7- 21 kPa, respectively [2, 74]. The toe and linear moduli for the human NP, extracted from the linear region of the stress-strain curve under unconfined compression, were reported as 3.2 ± 1.6 and 5.4 ± 2.6 kPa, respectively [75]. Using bovine IVDs, Recuerda et al. reported young's modulus (unconfined compression) of 190 ± 170 kPa for the NP [76]. The NP storage and loss moduli were reported as 64 ± 28 and 24 ± 11 kPa for ovine IVDs, respectively [77]. In addition, the average young's modulus for human AF single lamella was reported to be 45 ± 39 and 17 ± 6 MPa in the radial and circumferential directions of loading, respectively [56, 57, 63, 65, 73, 78-82]. The average tensile modulus for ovine, bovine, and porcine single lamella was reported as 0.47 ± 0.2, 1.9 ± 0.6, and 0.9 ± 0.3 MPa, respectively [83]. The young's modulus of the TZ in the current study was 0.31 (± 0.16) kPa which was significantly lower than the AF single lamella values (0.47 ± 0.2 MPa). The observation of lower mechanical properties for the TZ compared to the AF is likely relevant to

the structural parameters of the IVD fibrous components. The AF lamella consists of dense and highly packed collagen fibers that are intertwined with a well-organized network of elastic fibers. In contrast, the density of collagen and the thickness of elastic fibers in the TZ and NP are lower than in the AF [8, 48]. Other factors could be collagen inter-bundle connectivity, deformation, and mobility [71, 84], the nature of endplate-fibrous constituent assembly [62], and regional collagen fiber orientations that affect the IVD regional mechanical properties [85, 86]. A higher density of inter-bundle connectivity along with the presence of elastin cross-bridges within the AF may affect the regional tissue mobility and stiffness.

Detailed mechanical characterization of the TZ region in the IVD provides crucial information about the nature of the NP-AF integration, which has not been fully explored in the literature. Accordingly, due to the lack of relevant information, the mechanical characteristics of the TZ region have been rarely used in the development of IVD computational models and current IVD constitutive models have applied similar material properties to both the NP and the TZ [87-90]. In addition, integration and material properties gradient between the NP and AF are frequently ignored in the fabrication of tissue-engineered IVD scaffolds due to the lack of specific knowledge for the TZ zone [66, 91]. Therefore, the results of the current study may be used to develop more accurate IVD computational and realistic tissue-engineered models.

5. conclusion

The IVD structural integrity affects the mechanical properties; hence impacting IVD function. Indeed, microstructural damage, including the disruption of the AF lamellae and loss of connectivity between the IVD components, can affect IVD function. Of particular interest, the mechanical characterization of the TZ provides important information about how the AF and NP are connected. It is thought that the TZ region can tune the NP mobility during bulging which prevents proteoglycans from leaking out through the AF and therefore maintains the NP

hydration which is associated with the normal IVD function [5]. The current study identified the mechanical contribution of the TZ to the structural integrity of the IVD and provided fundamental information on the nature of NP-AF integration. The findings from this study revealed that the mechanical properties of the TZ region, including young's and toe moduli, maximum stress, failure strain, and toughness, were significantly lower for the PL compared to the AL region.

Acknowledgment:

Javad Tavakoli is grateful for the support of the University of Technology Sydney (UTS) with a Chancellor's Research Fellowship for the research work. In addition, Javad Tavakoli and Joanne L. Tipper thank AO Spine for their financial support through the AOSpine National Research Grant: AOSAUNZ(R) 2020-02.

References

[1] D.C. Keyes, E.L. Compere, The normal and pathological physiology of the nucleus pulposus of the intervertebral disc: an anatomical, clinical, and experimental study, JBJS 14(4) (1932) 897-938.
[2] J.C. Iatridis, M. Weidenbaum, L.A. Setton, V.C. Mow, Is the nucleus pulposus a solid or a fluid? Mechanical behaviors of the nucleus pulposus of the human intervertebral disc, Spine 21(10) (1996) 1174-1184.
[3] M. Humzah, R. Soames, Human intervertebral disc: structure and function, The Anatomical Record 220(4) (1988) 337-356.
[4] M. Sharabi, K.R. Wade, F. Galbusera, V. Rasche, R. Haj-Ali, H.-J. Wilke, Three-dimensional microstructural reconstruction of the ovine intervertebral disc using ultrahigh field MRI, The Spine Journal 18(11) (2018) 2119-2127.
[5] K.R. Wade, P.A. Robertson, N.D. Broom, On the extent and nature of nucleus-annulus integration, Spine (Phila Pa 1976) 37(21) (2012) 1826-33.
[6] L.J. Smith, N.L. Fazzalari, Regional variations in the density and arrangement of elastic fibres in the anulus fibrosus of the human lumbar disc, J Anat 209(3) (2006) 359-367.
[7] J. Yu, C. Peter, S. Roberts, J.P. Urban, Elastic fibre organization in the intervertebral discs of the bovine tail, J Anat 201(6) (2002) 465-475.
[8] J. Tavakoli, A.D. Diwan, J.L. Tipper, The ultrastructural organization of elastic fibers at the interface of the nucleus and annulus of the intervertebral disc, Acta Biomaterialia (2020).
[9] J.C. Salvatierra, T.Y. Yuan, H. Fernando, A. Castillo, W.Y. Gu, H.S. Cheung, C.-Y.C. Huant, Difference in energy metabolism of annulus fibrosus and nucleus pulposus cells of the intervertebral disc, Cellular and molecular bioengineering 4(2) (2011) 302.
[10] G.G. van den Akker, M.I. Koenders, F.A. van de Loo, P.L. van Lent, E.B. Davidson, P.M. van der Kraan, Transcriptional profiling distinguishes inner and outer annulus fibrosus from nucleus pulposus in the bovine intervertebral disc, European Spine Journal 26(8) (2017) 2053-2062.

[11] F. Guilak, H.P. Ting-Beall, A.E. Baer, W.R. Trickey, G.R. Erickson, L.A. Setton, Viscoelastic properties of intervertebral disc cells: identification of two biomechanically distinct cell populations, Spine 24(23) (1999) 2475.
[12] S. Roberts, J. Menage, J. Urban, Biochemical and structural properties of the cartilage end-plate and its relation to the intervertebral disc, Spine 14(2) (1989) 166-174.
[13] C. Hirsch, F. Schajowicz, Studies on structural changes in the lumbar annulus fibrosus, Acta Orthopaedica Scandinavica 22(1-4) (1952) 184-231.
[14] J. Tavakoli, J.J. Costi, A method for visualization and isolation of elastic fibres in annulus fibrosus of the disc, Materials Science and Engineering: C 93 (2018) 299-304.
[15] J. Tavakoli, A.D. Diwan, J.L. Tipper, Elastic Fibers: The Missing Key to Improve Engineering Concepts for Reconstruction of the Nucleus Pulposus in the Intervertebral Disc, Acta Biomaterialia (2020).
[16] N. Berger-Roscher, G. Casaroli, V. Rasche, T. Villa, F. Galbusera, H.-J. Wilke, Influence of Complex Loading Conditions on Intervertebral Disc Failure, Spine 42(2) (2017) E78-E85.
[17] K.R. Wade, P.A. Robertson, A. Thambyah, N.D. Broom, How healthy discs herniate: a biomechanical and microstructural study investigating the combined effects of compression rate and flexion, Spine 39(13) (2014) 1018-1028.
[18] S.P. Veres, P.A. Robertson, N.D. Broom, The Morphology of Acute Disc Herniation: A Clinically Relevant Model Defining the Role of Flexion, Spine 34(21) (2009) 2288-2296.
[19] K.R. Wade, M.L. Schollum, P.A. Robertson, A. Thambyah, N.D. Broom, A more realistic disc herniation model incorporating compression, flexion and facet-constrained shear: a mechanical and microstructural analysis. Part I: Low rate loading, European Spine Journal 26(10) (2017) 2616-2628.
[20] J. Tavakoli, D.B. Amin, B.J.C. Freeman, J.J. Costi, The Biomechanics of the Inter-Lamellar Matrix and the Lamellae During Progression to Lumbar Disc Herniation: Which is the Weakest Structure?, Ann Biomed Eng 46(9) (2018) 1280-1291.
[21] K.R. Wade, P.A. Robertson, A. Thambyah, N.D. Broom, “Surprise” Loading in Flexion Increases the Risk of Disc Herniation Due to Annulus-Endplate Junction Failure: A Mechanical and Microstructural Investigation, Spine 40(12) (2015) 891-901.
[22] V.M. van Heeswijk, A. Thambyah, P.A. Robertson, N.D. Broom, Posterolateral Disc Prolapse in Flexion Initiated by Lateral Inner Annular Failure: An Investigation of the Herniation Pathway, Spine (Phila Pa 1976) 42(21) (2017) 1604-1613.
[23] S. Rajasekaran, N. Bajaj, V. Tubaki, R.M. Kanna, A.P. Shetty, ISSLS Prize Winner: The Anatomy of Failure in Lumbar Disc Herniation: An: In Vivo:, Multimodal, Prospective Study of 181 Subjects, Spine 38(17) (2013) 1491-1500.
[24] D.B. Amin, J. Tavakoli, B.J.C. Freeman, J.J. Costi, Mechanisms of Failure Following Simulated Repetitive Lifting: A Clinically Relevant Biomechanical Cadaveric Study, Spine 45(6) (2020).
[25] J.E. Scott, T.R. Bosworth, A.M. Cribb, J.R. Taylor, The chemical morphology of age-related changes in human intervertebral disc glycosaminoglycans from cervical, thoracic and lumbar nucleus pulposus and annulus fibrosus, J Anat 184(Pt 1) (1994) 73.
[26] S. Kumaresan, N. Yoganandan, F. Pintar, M. Macias, J. Cusick, Morphology of young and old cervical spine intervertebral disc tissues, Biomedical sciences instrumentation 36 (2000) 141-146.
[27] K. Lundon, K. Bolton, Structure and function of the lumbar intervertebral disk in health, aging, and pathologic conditions, Journal of orthopaedic & sports physical therapy 31(6) (2001) 291-306.
[28] L.M. Benneker, P.F. Heini, S.E. Anderson, M. Alini, K. Ito, Correlation of radiographic and MRI parameters to morphological and biochemical assessment of intervertebral disc degeneration, European Spine Journal 14(1) (2005) 27-35.
[29] P. Ghosh, T. Taylor, B. Horsburgh, The composition and protein metabolism in the immature rabbit intervertebral disc, Cell and tissue research 163(2) (1975) 223-238.
[30] H.-J. Hansen, S. Ullberg, Uptake of S35 in the intervertebral discs after injection of S35-sulphate. An autoradiographic study, Acta Orthopaedica Scandinavica 30(1-4) (1961) 84-90.

[31] W. Souter, Sulphated acid mucopolysaccharide metabolism in the rabbit intervertebral disc. An autoradiographic study, Annals of the rheumatic diseases 30(2) (1971) 202.
[32] W.A. Souter, T.K. Taylor, Sulphated acid mucopolysaccharide metabolism in the rabbit intervertebral disc, The Journal of bone and joint surgery. British volume 52(2) (1970) 371-384.
[33] T. Taylor, P. Ghosh, G. Bushell, The contribution of the intervertebral disk to the scoliotic deformity, Clinical orthopaedics and related research (156) (1981) 79-90.
[34] J. Tavakoli, J.J. Costi, New findings confirm the viscoelastic behaviour of the inter-lamellar matrix of the disc annulus fibrosus in radial and circumferential directions of loading, Acta Biomater 71 (2018) 411-419.
[35] J. Tavakoli, J.J. Costi, New insights into the viscoelastic and failure mechanical properties of the elastic fiber network of the inter-lamellar matrix in the annulus fibrosus of the disc, Acta Biomaterialia 77 (2018) 292-300.
[36] D.S. Perie, J.J. Maclean, J.P. Owen, J.C. Iatridis, Correlating material properties with tissue composition in enzymatically digested bovine annulus fibrosus and nucleus pulposus tissue, Annals of biomedical engineering 34(5) (2006) 769-777.
[37] J.J. Costi, I.A. Stokes, M. Gardner-Morse, J. Laible, H.M. Scoffone, J. Iatridis, Direct measurement of intervertebral disc maximum shear strain in six degrees of freedom: motions that place disc tissue at risk of injury, Journal of biomechanics 40(11) (2007) 2457-2466.
[38] H.J. Wilke, P. Neef, M. Caimi, T. Hoogland, L.E. Claes, New in vivo measurements of pressures in the intervertebral disc in daily life, Spine 24(8) (1999) 755-762.
[39] A. Nachemson, J.M. Morris, In vivo measurements of intradiscal pressure: discometry, a method for the determination of pressure in the lower lumbar discs, JBJS 46(5) (1964) 1077-1092.
[40] D.B. Amin, D. Sommerfeld, I.M. Lawless, R.M. Stanley, B. Ding, J.J. Costi, Effect of degeneration on the six degree of freedom mechanical properties of human lumbar spine segments, Journal of Orthopaedic Research 34(8) (2016) 1399-1409.
[41] J.J. Costi, I.A. Stokes, M.G. Gardner-Morse, J.C. Iatridis, Frequency-dependent behavior of the intervertebral disc in response to each of six degree of freedom dynamic loading: solid phase and fluid phase contributions, Spine 33(16) (2008) 1731.
[42] L.J. Smith, S. Byers, J.J. Costi, N.L. Fazzalari, Elastic fibers enhance the mechanical integrity of the human lumbar anulus fibrosus in the radial direction, Ann Biomed Eng 36(2) (2008) 214-23.
[43] D.T. Pham, J.G. Shapter, J.J. Costi, Tensile behaviour of individual fibre bundles in the human lumbar anulus fibrosus, Journal of Biomechanics 67 (2018) 24-31.
[44] Y. Fujita, N.A. Duncan, J.C. Lotz, Radial tensile properties of the lumbar annulus fibrosus are site and degeneration dependent, Journal of Orthopaedic Research 15(6) (1997) 814-9.
[45] M.L. Schollum, P.A. Robertson, N.D. Broom, ISSLS prize winner: microstructure and mechanical disruption of the lumbar disc annulus: part I: a microscopic investigation of the translamellar bridging network, Spine (Phila Pa 1976) 33(25) (2008) 2702-10.
[46] N.L. Fazzalari, J.J. Costi, T.C. Hearn, R.D. Fraser, B. Vernon-Roberts, J. Hutchinson, B.A. Manthey, I.H. Parkinson, C. Sinclair, Mechanical and pathologic consequences of induced concentric anular tears in an ovine model, Spine 26(23) (2001) 2575-2581.
[47] H.-J. Wilke, A. Kettler, L.E. Claes, Are sheep spines a valid biomechanical model for human spines?, Spine 22(20) (1997) 2365-2374.
[48] G.D. O'Connell, E.J. Vresilovic, D.M. Elliott, Comparison of animals used in disc research to human lumbar disc geometry, Spine 32(3) (2007) 328-333.
[49] J. Tavakoli, D. Elliott, J. Costi, The ultra-structural organization of the elastic network in the intra- and inter-lamellar matrix of the intervertebral disc, Acta biomaterialia 58 (2017) 269-277.
[50] J. Tavakoli, J.J. Costi, Ultrastructural organization of elastic fibres in the partition boundaries of the annulus fibrosus within the intervertebral disc, Acta biomaterialia 68 (2018) 67-77.
[51] E.Y. Jiang, S.R. Sloan, C. Wipplinger, S. Kirnaz, R. Härtl, L.J. Bonassar, Proteoglycan removal by chondroitinase ABC improves injectable collagen gel adhesion to annulus fibrosus, Acta Biomaterialia 97 (2019) 428-436.

[52] J. Tavakoli, J.J. Costi, Development of a rapid matrix digestion technique for ultrastructural analysis of elastic fibers in the intervertebral disc, Journal of the mechanical behavior of biomedical materials 71 (2017) 175-183.
[53] Y. Moriguchi, B. Borde, C. Berlin, C. Wipplinger, S.R. Sloan, S. Kirnaz, B. Pennicooke, R. Navarro-Ramirez, T. Khair, P. Grunert, E. Kim, L. Bonassar, R. Härtl, In vivo annular repair using high-density collagen gel seeded with annulus fibrosus cells, Acta Biomaterialia 79 (2018) 230-238.
[54] J.P. Callaghan, S.M. McGill, Intervertebral disc herniation: studies on a porcine model exposed to highly repetitive flexion/extension motion with compressive force, Clinical Biomechanics 16(1) (2001) 28-37.
[55] L.J. Grobler, E.H. Simmons, T.W. Barrington, Intervertebral disc herniation in the adolescent, Spine 4(3) (1979) 267-278.
[56] E.R. Acaroglu, J.C. Latridis, L.A. Setton, R.J. Foster, V.C. Mow, M. Weidenbaum, Degeneration and aging affect the tensile behavior of human lumbar anulus fibrosus, Spine 20(24) (1995) 2690-2701.
[57] S. Ebara, J.C. Iatridis, L.A. Setton, R.J. Foster, V.C. Mow, M. Weidenbaum, Tensile properties of nondegenerate human lumbar anulus fibrosus, Spine 21(4) (1996) 452-461.
[58] T. Green, M. Adams, P. Dolan, Tensile properties of the annulus fibrosus, European Spine Journal 2(4) (1993) 209-214.
[59] F. Marchand, A.M. Ahmed, Investigation of the laminate structure of lumbar disc anulus fibrosus, Spine 15(5) (1990) 402-410.
[60] C. Pezowicz, Analysis of selected mechanical properties of intervertebral disc annulus fierosus in macro and microscopic scale, Journal of theoretical and applied mechanics 48(4) (2010) 917-932.
[61] C.A. Pezowicz, P.A. Robertson, N.D. Broom, The structural basis of interlamellar cohesion in the intervertebral disc wall, J Anat 208(3) (2006) 317-30.
[62] K.R. Wade, P.A. Robertson, N.D. Broom, A fresh look at the nucleus-endplate region: new evidence for significant structural integration, European Spine Journal 20(8) (2011) 1225-1232.
[63] H.A.L. Guerin, D.M. Elliott, Degeneration affects the fiber reorientation of human annulus fibrosus under tensile load, Journal of Biomechanics 39(8) (2006) 1410-1418.
[64] N.L. Nerurkar, D.M. Elliott, R.L. Mauck, Mechanical design criteria for intervertebral disc tissue engineering, Journal of biomechanics 43(6) (2010) 1017-1030.
[65] G.D. O'Connell, H.L. Guerin, D.M. Elliott, Theoretical and Uniaxial Experimental Evaluation of Human Annulus Fibrosus Degeneration, Journal of Biomechanical Engineering 131(11) (2009).
[66] S.E. Gullbrand, D.H. Kim, E. Bonnevie, B.G. Ashinsky, L.J. Smith, D.M. Elliott, R.L. Mauck, H.E. Smith, Towards the scale up of tissue engineered intervertebral discs for clinical application, Acta Biomaterialia 70 (2018) 154-164.
[67] S.E. Gullbrand, B.G. Ashinsky, E.D. Bonnevie, D.H. Kim, J.B. Engiles, L.J. Smith, D.M. Elliott, T.P. Schaer, H.E. Smith, R.L. Mauck, Long-term mechanical function and integration of an implanted tissue-engineered intervertebral disc, Science Translational Medicine 10(468) (2018) eaau0670.
[68] M. Sharabi, S. Wertheimer, K.R. Wade, F. Galbusera, D. Benayahu, H.-J. Wilke, R. Haj-Ali, Towards intervertebral disc engineering: Bio-mimetics of form and function of the annulus fibrosus lamellae, Journal of the Mechanical Behavior of Biomedical Materials 94 (2019) 298-307.
[69] M. Sharabi, K. Wade, R. Haj-Ali, The mechanical role of collagen fibers in the intervertebral disc, Biomechanics of the Spine (2018) 105-123.
[70] F. Ghezelbash, A.H. Eskandari, A. Shirazi-Adl, M. Kazempour, J. Tavakoli, M. Baghani, J.J. Costi, Modeling of human intervertebral disc annulus fibrosus with complex multi-fiber networks, Acta Biomaterialia 123 (2021) 208-221.
[71] C.M. Disney, A. Eckersley, J.C. McConnell, H. Geng, A.J. Bodey, J.A. Hoyland, P.D. Lee, M.J. Sherratt, B.K. Bay, Synchrotron tomography of intervertebral disc deformation quantified by digital volume correlation reveals microstructural influence on strain patterns, Acta Biomaterialia 92 (2019) 290-304.

[72] J. Tavakoli, D.M. Elliott, J.J. Costi, Structure and mechanical function of the inter-lamellar matrix of the annulus fibrosus in the disc, Journal of Orthopaedic Research 34(8) (2016) 1307-1315.
[73] G.A. Holzapfel, C.A. Schulze-Bauer, G. Feigl, P. Regitnig, Single lamellar mechanics of the human lumbar anulus fibrosus, Biomechanics and modeling in mechanobiology 3(3) (2005) 125-140.
[74] W. Johannessen, D.M. Elliott, Effects of degeneration on the biphasic material properties of human nucleus pulposus in confined compression, Spine (Phila Pa 1976) 30(24) (2005) E724-9.
[75] J.M. Cloyd, N.R. Malhotra, L. Weng, W. Chen, R.L. Mauck, D.M. Elliott, Material properties in unconfined compression of human nucleus pulposus, injectable hyaluronic acid-based hydrogels and tissue engineering scaffolds, Eur Spine J 16(11) (2007) 1892-1898.
[76] M. Recuerda, D. Périé, G. Gilbert, G. Beaudoin, Assessment of mechanical properties of isolated bovine intervertebral discs from multi-parametric magnetic resonance imaging, BMC Musculoskeletal Disorders 13(1) (2012) 195.
[77] J.C. Leahy, D.W.L. Hukins, Viscoelastic properties of the nucleus pulposus of the intervertebral disk in compression, Journal of Materials Science: Materials in Medicine 12(8) (2001) 689-692.
[78] J.L. Isaacs, E. Vresilovic, S. Sarkar, M. Marcolongo, Role of biomolecules on annulus fibrosus micromechanics: effect of enzymatic digestion on elastic and failure properties, J Mech Behav Biomed Mater 40 (2014) 75-84.
[79] R.G. Long, O.M. Torre, W.W. Hom, D.J. Assael, J.C. Iatridis, Design requirements for annulus fibrosus repair: review of forces, displacements, and material properties of the intervertebral disk and a summary of candidate hydrogels for repair, Journal of biomechanical engineering 138(2) (2016) 021007.
[80] D. Skaggs, M. Weidenbaum, J.C. Iatridis, A. Ratcliffe, V.C. Mow, Regional variation in tensile properties and biochemical composition of the human lumbar anulus fibrosus, Spine 19(12) (1994) 1310-1319.
[81] B.D. Stemper, J.L. Baisden, N. Yoganandan, B.S. Shender, D.J. Maiman, Mechanical yield of the lumbar annulus: a possible contributor to instability, Journal of Neurosurgery: Spine 21(4) (2014) 608-613.
[82] D.M. Elliott, L.A. Setton, Anisotropic and inhomogeneous tensile behavior of the human anulus fibrosus: experimental measurement and material model predictions, Journal of biomechanical engineering 123(3) (2001) 256-263.
[83] L.A. Monaco, S.J. DeWitte-Orr, D.E. Gregory, A comparison between porcine, ovine, and bovine intervertebral disc anatomy and single lamella annulus fibrosus tensile properties, Journal of morphology 277(2) (2016) 244-251.
[84] C. Vergari, J. Mansfield, J.R. Meakin, P.C. Winlove, Lamellar and fibre bundle mechanics of the annulus fibrosus in bovine intervertebral disc, Acta Biomater 37 (2016) 14-20.
[85] A.J. Michalek, M.R. Buckley, L.J. Bonassar, I. Cohen, J.C. Iatridis, Measurement of local strains in intervertebral disc anulus fibrosus tissue under dynamic shear: contributions of matrix fiber orientation and elastin content, J Biomech 42(14) (2009) 2279-85.
[86] C.M. Disney, J. Mo, A. Eckersley, A.J. Bodey, J.A. Hoyland, M.J. Sherratt, A.A. Pitsillides, P.D. Lee, B.K. Bay, Regional variations in discrete collagen fibre mechanics within intact intervertebral disc resolved using synchrotron computed tomography and digital volume correlation, Acta Biomaterialia 138 (2022) 361-374.
[87] N.T. Jacobs, D.H. Cortes, J.M. Peloquin, E.J. Vresilovic, D.M. Elliott, Validation and application of an intervertebral disc finite element model utilizing independently constructed tissue-level constitutive formulations that are nonlinear, anisotropic, and time-dependent, Journal of biomechanics 47(11) (2014) 2540-2546.
[88] A. Malandrino, J.A. Planell, D. Lacroix, Statistical factorial analysis on the poroelastic material properties sensitivity of the lumbar intervertebral disc under compression, flexion and axial rotation, J Biomech 42(16) (2009) 2780-8.

[89] I.A. Stokes, J.P. Laible, M.G. Gardner-Morse, J.J. Costi, J.C. Iatridis, Refinement of elastic, poroelastic, and osmotic tissue properties of intervertebral disks to analyze behavior in compression, Ann Biomed Eng 39(1) (2011) 122-31.
[90] Y. Schroeder, W. Wilson, J.M. Huyghe, F.P.T. Baaijens, Osmoviscoelastic finite element model of the intervertebral disc, European Spine Journal 15(3) (2006) 361.
[91] Q. Yang, H.-w. Xu, S. Hurday, B.-s. Xu, Construction Strategy and Progress of Whole Intervertebral Disc Tissue Engineering, Orthopaedic Surgery 8(1) (2016) 11-18.